can be explained by two competing mechanisms: the strain hardening effect increasing the yield strength and the Bauschinger effect causing a yield strength drop.

Discussing the Bauschinger effect first, it is much larger in the A steel than in the B steel, and thus, the yield strength drop in the A steel is twice that of the B steel (43 MPa *vs* 22 MPa) under the strain of piping (Figure 5). This yield strength drop can be explained by the pinning of mobile dislocations due to the presence of fine Nb(C,N) carbonitrides, as suggested by Seeger *et al.*[11] In the A steel, Ti(C,N) carbonitrides due to the Ti addition here additionally promote the dislocation pinning, thereby leading to the larger Bauschinger effect. On the other hand, the strain hardening effect is much larger in the B steel than in the A steel, as shown in the stress-strain curves of Figure 4. This is because considerable strain hardening occurs in the B steel under the 1.4 pct strain applied during piping, whereas almost no strain hardening results from the 1.6 pct strain in the A steel. This difference in strain hardening of the two steels is attributed to the presence or absence of a yield-point phenomenon. The B steel undergoes considerable strain hardening under strains as small as 1.4 pct because of its continuous yielding behavior, whereas the A steel hardly has any strain hardening because of the yield-point phenomenon. This yield-point phenomenon is also associated with alloy compositions and microstructures. According to Coldren *et al.*[12,13] and Irani and Tither[14] by adding molybdenum into HSLA steels, the $\gamma \rightarrow \alpha$ transformation temperature can be lowered, pearlite formation can be discouraged, and low-temperature transformation products such as acicular ferrite having high dislocation density can be promoted. Because of this high density of mobile dislocations, the yield-point phenomenon does not occur as the movement of dislocations under an applied stress gradually increases and the elastic limit decreases. In this study, the Mo-containing B steel has formed acicular ferrite having high density of dislocations (Figure 3(c)) and is, accordingly, confirmed to have the lower yield strength and the continuous yielding behavior (Figure 4 and Table III). Consequently, in the A steel, the Bauschinger effect after piping is larger due to the precipitation of fine carbonitrides, but little strain hardening occurs because of the yield-point phenomenon. With the Bauschinger effect overriding the strain hardening effect, the yield strength is significantly reduced. On the other hand, since the B steel shows the continuous yielding behavior due to the Mo addition, the strain hardening effect becomes larger, enough to offset the Bauschinger effect. Thus, the yield strength after piping increases rather than drops.

These findings present that two competing mechanisms, *i.e.*, the strain hardening effect increasing the yield strength and the Bauschinger effect decreasing it, are operating and explain the yield strength variations occurring in API-X70 steel plates after piping. Particularly, capitalizing on the fact that the absence of the yield-point phenomenon is associated with the larger strain hardening effect, Mo was added to eliminate or to reduce the yield-point phenomenon. This proves useful in preventing the reduction of yield strength and increases it. In evaluating pipe formability, investigations of the tensile properties including the yield-point phenomenon provide valuable data in addition to the evaluation of the Bauschinger effect.

This work has been supported by 1997 Pohang Iron and Steel Co. (POSCO) under Contract No. 1PD9704001. The authors thank Professor Nack J. Kim, POSTECH; Dr. Ki Jong Park, Dr. Kwang Sup Noh, and Mr. Jung Min Choi, POSCO; and Mr. Jae Eul Kim, Mijoo Steel Co., for their helpful discussion on spiral piping and macrostructural analysis.

REFERENCES

1. R.W.K. Honeycombe: *Scand. J. Metall.*, 1956, vol. 8, pp. 21-26.
2. H. Watanabe, Y.E. Smith, and R.D. Pejlke: *The Hot Deformation of Austenite*, AIME, New York, NY, 1997, pp. 140-68.
3. *Specification for High-Test Linepipe*, 18th ed., American Petroleum Institute, Standard 5XL, New York, 1971.
4. Material Specification, Canadian Arctic Gas Pipeline Limited, Specification No. 2950-6-6, 1973.
5. G.E. Dieter: *Mechanical Metallurgy*, 3rd ed., McGraw-Hill, New York, NY, 1986, pp. 236-37.
6. R. Sowerby, Y. Tomita, and D.K. Uko: *Mater. Sci. Eng.*, 1979, vol. 41, pp. 43-58.
7. T. Taira, T. Osuka, and Y. Ishida: *Proc. 15th Mechanical Working and Steel Processing Conf.*, Pittsburgh, PA, 1977, p. 33.
8. G. Tither and M. Lavite: *J. Met.*, 1975, vol. 27, pp. 15-23.
9. K.J. Pascoe: *J. Strain Analysis*, 1971, vol. 6, pp. 167-80.
10. C.D. Singh and V. Ramaswamy: *Steel India*, 1983, vol. 6, pp. 89-98.
11. A. Seeger, S. Mader, and H. Kranmuller: *Interscience*, 1963, p. 665.
12. A.P. Coldren, Y.E. Smith, and R.L. Cryderman: *Processing and Properties of Low-Carbon Steel*, AIME, New York, NY, 1973, pp. 163-89.
13. A.P. Coldren and J.L. Mehelich: *Molybdenum Containing Steels for Gas and Oil Industry Application*, Climax Molybdenum Co., Greenwich, CN, 1977, pp. 14-28.
14. J.J. Irani and G. Tither: *ISI Publication*, 1967, vol. 104, p. 135.

Measurement of the Activity of Boron in Liquid Copper using a Four-Phase Equilibrium Technique

K.T. JACOB, SHASHANK PRIYA, and YOSHIO WASEDA

Boron can be used to deoxidize liquid copper. It can be added as a Cu-B master alloy or as tetraboron carbide ($B_{4+x}C$). Presence of boron as a minor element is known to increase the resistance of copper alloys to corrosive wear. Despite potential application in the metallurgy of copper, there is no reliable experimental information on either the activity of boron in liquid copper or of its effect on the behavior of dissolved oxygen.

The phase diagram of Cu-B system is of simple eutectic type characterized by eutectic temperature of 1286 K and eutectic composition $X_B = 0.133$.[1] Phase diagram literature has been reviewed by Chakrabarti and Laughlin.[1] There is some uncertainty in the reported values for the eutectic temperature and composition.

K.T. JACOB, Professor, Department of Metallurgy and Materials Research Center, and SHASHANK PRIYA, Graduate Student, Department of Metallurgy, are with the Indian Institute of Science, Bangalore 560 012, India. YOSHIO WASEDA, Professor and Director, is with the Institute for Advanced Materials Processing, Tohoku University, Sendai 980-8577, Japan.

Manuscript submitted October 29, 1999.

Yukinobu *et al.*[2] have determined the activity of boron in liquid Cu-B alloys at low concentrations by electromotive force measurement. A cell incorporating calcium aluminoborate melt as the electrolyte was used. The activities exhibit large positive deviation from Raoult's law. Batalin *et al.*[3] have determined partial and integral enthalpy of mixing of the liquid Cu-B alloys in the Cu-rich region at 1790 K by high-temperature calorimetry using high purity copper and amorphous boron as starting materials. Their values for partial enthalpy of boron at low concentrations show large scatter. From their results, the partial heat of mixing of boron at infinite dilution in liquid Cu-B alloys can be estimated as $57.57(\pm 20)$ kJ·mol^{-1} using the subregular solution model. Witusiewicz,[4] using an isoperibol high-temperature calorimeter, has investigated the thermodynamic properties of liquid Cu-B alloys. A value of $45(\pm 10)$ kJ·mol^{-1} for the partial enthalpy of mixing of boron at infinite dilution in liquid Cu-B alloys relative to solid boron as the standard state was obtained.

The purpose of this article is to report measurements on dilute Cu-B alloys at 1723 K using a new four-phase equilibrium technique. The method can be considered as an extension of the conventional procedure involving metal-slag-gas equilibration, where the gas phase containing carbon monoxide is pre-equilibrated with graphite to define the carbon and oxygen chemical potentials. Under the reducing atmosphere, liquid diboron trioxide (B_2O_3) is partially reduced by graphite generating a liquid Cu-B alloy and carbon monoxide at controlled pressure. After quenching to room temperature, the concentration of B in the liquid copper is measured. The equilibrium boron concentration in copper is measured as a function of the partial pressure of carbon monoxide in the gas phase.

High purity materials (Cu $>$ 99.999 mass pct, B_2O_3 $>$ 99.99 mass pct, CO $>$ 99.99 pct purity, and graphite of spectral grade) are used. B_2O_3 was dried first in flowing Ar for 8 hours at 423 K and then under vacuum at 473 K for 4 hours before use. Mixtures of Ar + CO of the desired composition are prepared by mixing metered streams of Ar and CO in a chamber filled with glass beads. Mass flow controllers are used to measure the flow rates accurately.

A schematic diagram of the apparatus used for measurement is shown in Figure 1. Liquid copper is held in a graphite crucible covered by a layer of liquid B_2O_3 melt. Carbon monoxide or a controlled mixture of Ar + CO is passed over the melt. In preliminary experiments, deposition of carbon was observed in the cooler parts of the vertical alumina tube in which the crucible was placed. Since the carbon deposition generates CO_2 in the gas phase and affects the oxygen potential, the gas phase is re-equilibrated with graphite by passing the gas through a chamber containing graphite chips maintained at the temperature of measurement. A rotating stirrer allows mixing of the metal and slag and accelerates the attainment of equilibrium between the gas and condensed phases. Although the equilibrium is attained in 1.5 hours at 1723 K, the system is maintained at the temperature with stirring for 2.5 hours. After passing over the melt, the gas exits the constant temperature zone through a small orifice in the graphite plug placed below the crucible. The deposition of carbon at furnace exit therefore does not alter the partial pressure of carbon monoxide in the high-temperature zone. The temperature of the metal and slag is measured by

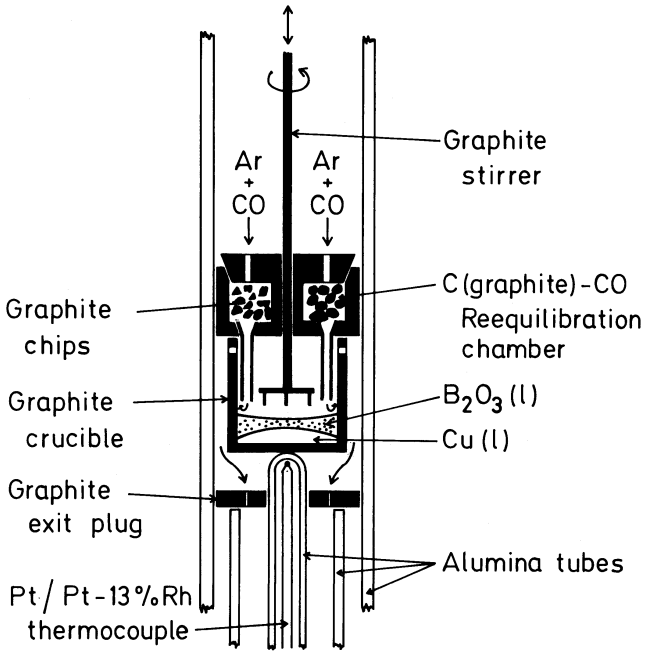

Fig. 1—Schematic diagram of the apparatus.

Table I. Equilibrium Boron Concentration in Liquid Copper at Different Partial Pressure of Carbon Monoxide in the Gas Phase and Derived Activity at 1723 K

p_{CO}/p°	X_B	$a_{B(s)}$
1.001	0.0222	0.0757
0.886	0.0262	0.0883
0.775	0.0333	0.1097
0.679	0.0416	0.1336
0.575	0.0568	0.1746
0.471	0.0779	0.226
0.429	0.0975	0.2696
0.387	0.118	0.3108

$p^\circ = 1.013 \times 10^5$ Pa (standard pressure).

a Pt/Pt − 13 pct Rh thermocouple, checked against the melting point of gold. An alumina tube protects the thermocouple. The temperature of the vertical resistance furnace is controlled to ±1 K.

The alumina tube enclosing the reaction chamber is closed at both ends by brass caps with provision for gas ports, stirrer, and thermocouple protection tube. The lower part of the alumina tube is water cooled. After 2.5 hours of equilibration, the stirrer is withdrawn, and metal and slag phase are allowed to separate for 0.5 hours. At the end of each experiment, the crucible is lowered into the water-cooled region. The concentration of boron in copper is determined using inductively-coupled plasma–emission spectrometer. The approach to equilibrium at constant partial pressure of CO is verified from both higher and lower concentrations of boron in liquid copper. Analysis of the slag phase indicated that the concentration of copper in the melt was below the detection level.

The equilibrium concentration of boron in copper at 1723 K at different partial pressures of carbon monoxide in the gas phase is shown in Table I. The same value for the

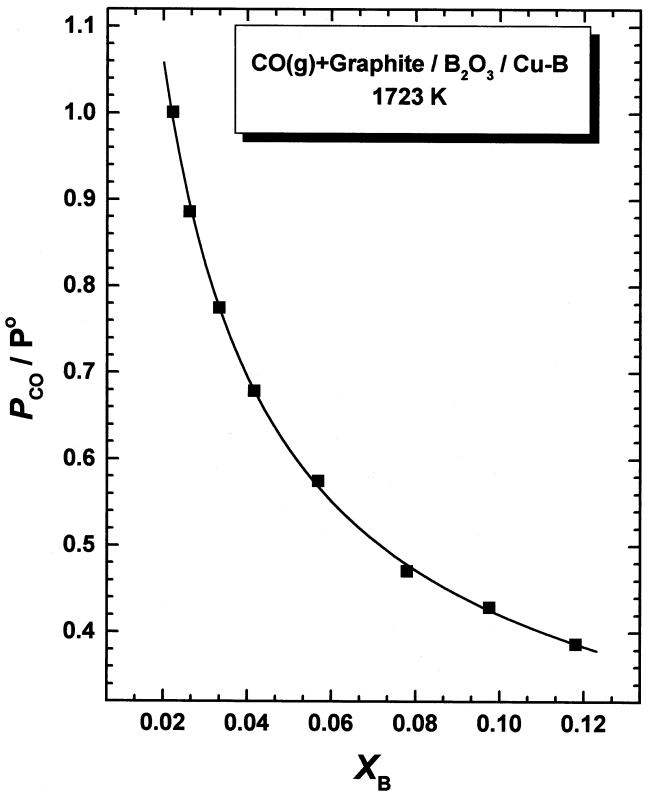

Fig. 2—Plot of the partial pressure of carbon monoxide as a function of composition of boron in liquid Cu in equilibrium with liquid B_2O_3 and graphite at 1723 K.

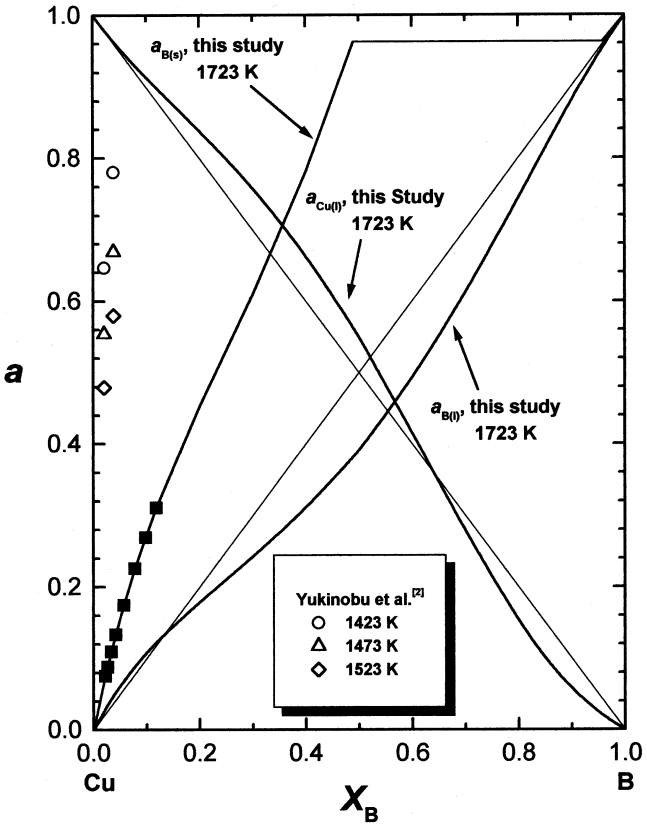

Fig. 3—Variation of the activity of boron and copper as a function of composition at 1723 K.

concentration of boron in liquid copper is obtained by approaching equilibrium from higher and lower partial pressures of CO. The partial pressure of CO is plotted as a function of alloy composition in Figure 2 at 1723 K. The formation of tetraboron carbide ($B_{4+x}C$) was encountered at lower partial pressures of CO. The reduction reaction can be written as

$$B_2O_3\ (l) + 3C\ (\text{graphite}) \rightarrow 3CO\ (g) + 2\underline{B}_{Cu} \qquad [1]$$

The activity of the boron in Cu-B alloy with respect to solid boron can be calculated from the Gibbs energy change for reaction [1]:

$$\Delta G^{\circ}_{[1]}\ (1723\ K) = -\ RT \ln K_{[1]} = -RT \ln (a^2_{B(s)} \cdot p^3_{CO}) \qquad [2]$$

where $a_{B(s)}$ is the activity of boron in the liquid alloy relative to solid boron as the standard state, p_{CO} is the partial pressure of CO, and $K_{[1]} = 5.60 \times 10^{-3}$ [5] is the equilibrium constant for the reaction at 1723 K. The computed values of $a_{B(s)}$ from Eq. [2] are given in Table I. The activity of boron in Cu-B alloy relative to liquid boron as the standard state can be calculated from the relation

$$RT \ln a_{B(l)} = RT \ln a_{B(s)} - (\mu^{\circ}_{B(l)} - \mu^{\circ}_{B(s)}) \qquad [3]$$

where $a_{B(l)}$ is the activity of boron in liquid alloy relative to liquid boron as the standard state, and $\mu^{\circ}_{B(l)} - \mu^{\circ}_{B(s)}$ is the difference in chemical potential for pure boron in solid and liquid states. The value of $\mu^{\circ}_{B(l)} - \mu^{\circ}_{B(s)}$ at 1723 K is computed using data for the pure element boron from Knacke *et al.*[5] The constant value given in the tables for the heat capacity of the liquid above the melting point is also used for the supercooled state. The Gibbs energies of fusion at 1723 K for Cu and boron are −3511 and 13,225 J mol^{-1}, respectively.[5] The activity of B is plotted as a function of composition in Figure 3 with respect to both solid and liquid boron as the standard states. The activity of boron relative to solid boron reported by Yukinobu *et al.*[2] in the temperature from 1423 to 1523 K, using a cell with molten calcium alumino-silicate as the electrolyte, is also shown for comparison. After correcting for the difference in temperature, the activities reported by Yukinobu *et al.* appear to be 70 pct higher than those obtained in this study. Yukinobu *et al.* have also measured activities in Fe-B and Co-B alloys using the same technique. Their values for the activity of boron in the Fe-B system are significantly higher than those critically assessed by Chart.[6] It is likely that the alumina-saturated calcium alumino-silicate melt used as the electrolyte is not a pure ionic conductor. Presence of some electronic conductivity can explain the higher activities of boron obtained by Yukinobu *et al.*

The function α_B defined as

$$\alpha_B = RT \ln \gamma_{B(l)}/(1 - X_B)^2 = \Delta G^E_{B(l)}/(1 - X_B)^2 \qquad [4]$$

is plotted as a function of composition of the liquid alloy in Figure 4. The activity coefficient of boron $\gamma_{B(l)}$ is calculated with reference to pure liquid boron. The values of α_B can be represented by a linear equation:

$$\alpha_B = 5418 - 38{,}849\ X_B\ (\pm 500) \qquad [5]$$

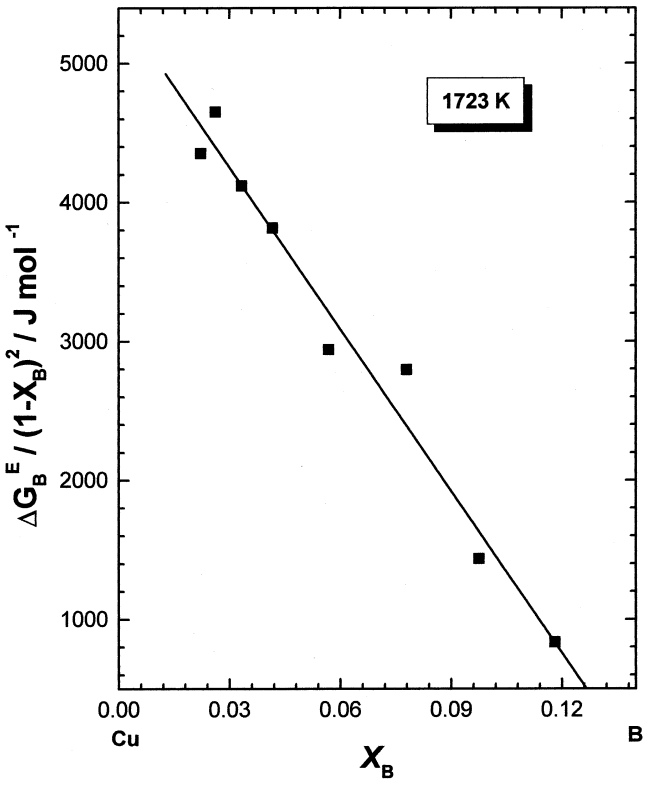

Fig. 4—Composition dependence of the α function at 1723 K. The standard state for B is pure liquid.

The uncertainty corresponds to twice the standard error estimate. The excess chemical potential or excess partial molar Gibbs energy of B at 1723 K with reference to pure liquid boron as the standard state is obtained from the expression for α_B:

$$\Delta\mu_B^E = \Delta G_B^E = RT \ln \gamma_{B(l)} = (1 - X_B)^2 \, [5418 - 38{,}849\, X_B] \text{ J mol}^{-1} \quad [6]$$

Although the equation is obtained from measurements on alloys with $X_B < 0.12$, it may be extrapolated up to phase boundary in the absence of other information. From the Gibbs—Duhem equation, the excess chemical potential of Cu and the integral excess Gibbs energy of mixing of liquid Cu-B alloys are obtained:

$$\Delta\mu_{Cu}^E = \Delta G_{Cu}^E = RT \ln \gamma_{Cu} = (X_B)^2 \, [24{,}843 - 38{,}849\, X_B] \text{ J mol}^{-1} \quad [7]$$

$$\Delta G^E = X_B\,(1 - X_B)\,[5418 - 19{,}424\, X_B] \text{ J mol}^{-1} \quad [8]$$

The system exhibits positive values for excess Gibbs energy of mixing for copper-rich alloys and negative values at higher concentrations of boron.

To obtain the temperature dependence of the excess Gibbs energy, the ratio (τ) of enthalpy to excess entropy of mixing was estimated as 4000 K. According to the correlation of Kubaschewski,[7]

$$\frac{\Delta H^M}{\Delta S^E} = 0.7813\,(T_A^b + T_B^b) \quad [9]$$

where T_A^b and T_B^b are the boiling points of pure metals A and B, ΔH^M and ΔS^E are the extremum values for enthalpy and excess entropy of mixing, the value of τ for the Cu-B system is 5450 K. Subsequently, Kubashewski[8] proposed that the ratio between partial enthalpy and partial excess entropy of solute elements in dilute solutions is 3400 K. Lupis and Elliot[9] have also proposed a similar relationship and a value of τ equal to 3000($\pm$1000) K. Using τ = 4000 K, the excess Gibbs energy can be partitioned into enthalpy and entropy terms. The partial enthalpy of boron at infinite dilution at 1790 K obtained by this procedure is 58.6 kJ·mol^{-1}, which is in fair agreement with the calorimetric values reported by Batalin *et al.*[3] and Witusiewicz,[4] considering their experimental uncertainties.

The chemical potential of each component at solidus composition is equal to its chemical potential at the liquidus at constant temperature and pressure: $\mu_B^s = \mu_B^l$ and $\mu_{Cu}^s = \mu_{Cu}^l$. Expressing the chemical potentials in the solid and liquid phases as a sum of ideal and excess components, one obtains the following equations containing two unknown compositions:

$$\ln\left(\frac{X_B^l}{X_B^s}\right) = \left(\frac{\mu_{B(s)}^0 - \mu_{B(l)}^0}{RT}\right) + \left(\frac{\Delta G_{B(s)}^E - \Delta G_{B(l)}^E}{RT}\right) \quad [10]$$

$$\ln\left(\frac{(1 - X_B^l)}{(1 - X_B^s)}\right) = \left(\frac{\mu_{Cu(s)}^0 - \mu_{Cu(l)}^0}{RT}\right) + \left(\frac{\Delta G_{Cu(s)}^E - \Delta G_{Cu(l)}^E}{RT}\right) \quad [11]$$

where X_B^s and X_B^l are the mole fractions of B at the solidus and liquidus at temperature T and ΔG_i^E is the relative excess partial Gibbs energy of mixing of the component i (Cu or B) in the solid and liquid Cu-B alloys. Values for the difference in chemical potential for pure copper and boron in solid and liquid states are computed from the data given in the compilation of Knacke *et al.*[5] The constant value given for the heat capacity of the liquid above the melting point is also used for the supercooled state. The enthalpy of fusion and melting points of pure metals used in the computation are as follows.

Element	ΔH_{fus}^0/J mol^{-1}	T_m/K
Cu	13,137	1358
B	50,199	2365

The lattice stabilities of B in the fcc structure are taken from Teppo and Taskinen:[10]

$$G_{B(fcc)}^0 - G_{B(rho)}^0 = 43{,}516 - 11.607T \quad \text{J mol}^{-1} \quad [12]$$

The lattice stability of Cu in the rhombohedral structure is estimated as

$$G_{Cu(rho)}^0 - G_{Cu(fcc)}^0 = 22{,}000 - 5T \quad \text{J mol}^{-1} \quad [13]$$

where the subscript rho represents the phase with rhombohedral structure.

The two terminal solid solutions were assumed to be regular, and excess Gibbs energy is defined by

$$\Delta G^E = X_B\,(1 - X_B)(34{,}765) \quad \text{J mol}^{-1} \quad [14]$$

for the Cu-rich solid solution with fcc structure, and

$$\Delta G^E = X_B\,(1 - X_B)(24{,}000) \quad \text{J mol}^{-1} \quad [15]$$

for the B-rich rhombohedral solid solution. The solidus and

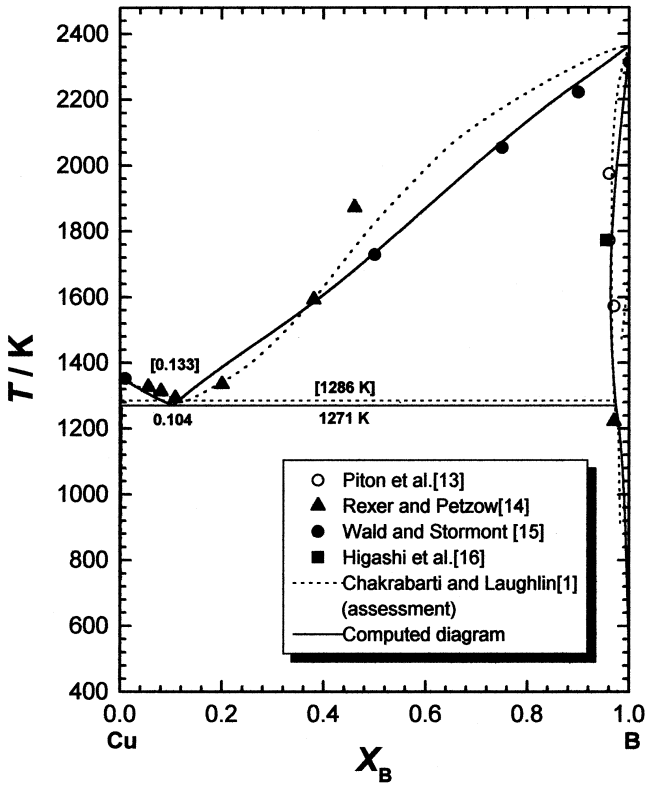

Fig. 5—Computed phase diagram for the system Cu-B. The dotted line shows the diagram reported in the current ASM compilation. The experimental data are also shown.

liquidus compositions at selected temperatures are obtained by solving Eqs. [10] and [11] using an iterative procedure. The solidus shows retrograde behavior at the boron-rich end. Varamban and Jacob[11] have recently discussed the retrograde solubility in semiconductors. The condition for inducing retrograde solubility is

$$\Omega_{\text{rho}} > \Delta H^{\text{o},f}_{\text{Cu}} + \Delta H^{\text{o},f}_{\text{B}} \left(\frac{X^{\text{liq}}_{\text{B}}}{X^{\text{liq}}_{\text{Cu}}} \right)_{\text{eut}} \qquad [16]$$

where Ω_{rho} is the enthalpy parameter of a pseudoregular solution for the B-rich solid solution. The expression was derived assuming liquid solution as ideal, and the solid solution exhibits symmetric enthalpy and excess entropy of mixing. The parameters used in this study satisfy Eq. [16].

The computed phase diagram is shown in Figure 5. The dotted lines show the phase diagram reported in the recent ASM compilation.[12] On the same diagram, available experimental information is also shown for comparison.[13–16] The phase diagram agrees well with the reported data. The calculated eutectic temperature and composition are $T_E = 1271$ K and $X_B = 0.103$. The terminal solubility of copper in boron at eutectic is 2.63 at. pct B and of boron in copper is 0.24 at. pct B. Thus, the phase diagram computed from the results obtained in this study is consistent with information available in the literature.

REFERENCES

1. D.J. Chakrabarti and D.E. Laughlin: *Bull. Alloy Phase Diagrams*, 1982, vol. 3, pp. 45-48.
2. M. Yukinobu, O. Ogawa, and S. Goto: *Metall. Trans. B*, 1989, vol. 20B, pp. 705-10.
3. G.I. Batalin, V.S. Sudavtsova, and M.V. Mikhailovskaya: *Sov. Nonferrous Met. Res.*, 1985, vol. 13, pp. 177-79.
4. V.T. Witusiewicz: *J. Alloys Compounds*, 1994, vol. 203, pp. 103-16.
5. O. Knacke, O. Kubashewski, and K. Hesselman: *Thermochemical Properties of Inorganic Substances*, 2nd ed., Springer-Verlag, Berlin, 1991, vols. I and II.
6. T.G. Chart: *Critical Assessment of Thermodynamic Data for the Iron-Boron System*, National Physical Laboratory of United Kingdom, Middlesex, United Kingdom, 1982.
7. O. Kubaschewski: *Phase Stability in Metals and Alloys*, P. Rudman, J. Stringer, and R. I. Jafee, eds., McGraw-Hill, New York, NY, 1967.
8. O. Kubashewski: *High Temp. High Pressure*, 1981, vol. 13, pp. 435-40.
9. C.H.P. Lupis and J.F. Elliot: *Acta Metall.*, 1967, vol. 15, pp. 265-76.
10. O. Teppo and P. Taskinen: *Mater. Sci. Technol.*, 1993, vol. 9, pp. 205-12.
11. S.V. Varamban and K.T. Jacob: *Metall. Mater. Trans. A*, 1998, vol. 29A, pp. 1525-27.
12. *Binary Alloy Phase Diagrams*, 2nd ed., T.B. Massalski, P.R. Subraminian, H. Okamoto, and L. Kaoprazak, eds., ASM INTERNATIONAL, Materials Park, OH, 1990.
13. J.P. Piton, G. Vuillard, and T. Lundstrom: *C.R. Acad. Sci., Ser. C*, 1974, vol. 278, pp. 1495-96.
14. J. Rexer and G. Petzow: *Metall.*, 1970, vol. 24, pp. 1083-86.
15. F. Wald and R. Stormont: *J. Less-Common Met.*, 1965, vol. 9, pp. 423-33.
16. I. Higashi, Y. Takahashi, and T. Atoda: *J. Less-Common Met.*, 1974, vol. 37, pp. 199-204.

An Oscillatory Behavior of Planar Interface Motion in the Naphthalene - Camphor System

L.M. FABIETTI

During directional solidification of alloys, the time-dependent phenomenon plays a crucial role in governing the microstructure evolution process and in the redistribution of solute.[1] During the growth of a planar interface at a fixed external velocity, the rejected solute (for solute distribution coefficient <1) builds up a boundary layer of solute near the interface, and the interface velocity is initially zero and approaches the external velocity when steady-state growth occurs. The dynamics of the interface velocity during this transient process are important, and they are controlled by two time-dependent phenomena: (1) the changes in the interface composition in the liquid with time, $\partial C_l/\partial t$, and (2) the change in the boundary layer thickness with time, $\partial \delta/\partial t$.

When local equilibrium is present at the interface, the preceding considerations predict that the velocity of the planar interface will increase continuously or the location of the interface will advance smoothly with time. This has been verified experimentally by the author in the succinonitrile-acetone system.[2] However, when the velocity is examined in the transient regime for a faceted material, where local equilibrium is not present, discontinuous growth of the interface motion is observed. The aim of this communication is to present these experimental results on the dynamics of faceted interface motion.

L.M. FABIETTI, Assistant Professor and Researcher of Conicet, is with the Facultad of Mathematics Astronomy and Physics, Universidad Nacional of Cordoba, 5000 Cordoba, Argentina.

Manuscript submitted December 29, 1999.